Spectral Estimation of Weak Signals with Strong Interference via Modulo Sampling

Shoaib Ahmed, Cengcang Zeng, and Hongbin Li
Department of Electrical and Computer Engineering
Stevens Institute of Technology
Hoboken, NJ 07030, USA

***Abstract*—This paper introduces a framework for spectral analysis of weak signals in the presence of strong interference that can potentially exceed the dynamic range of the analog-to-digital converter (ADC) employed for data acquisition. The framework combines modulo sampling to avoid ADC saturation with interference cancellation (IC) and adaptive spectral estimators such as amplitude and phase estimation of a sinusoid (APES) and Capon for high-resolution spectral analysis. Numerical simulations validate the proposed approach's ability to accurately recover weak signals' spectrum with significantly lower mean-squared error (MSE) in amplitude estimation compared to conventional methods in the considered scenarios. Notably, it is shown that APES and Capon are able to effectively reject the out-of-range interference and reveal weak spectral content, without requiring the interference cancellation step.**

***Index Terms*—Weak signal, strong interference, ADC saturation, modulo sampling, adaptive spectral estimator**

I. Introduction

Advanced spectral estimation techniques play an important role in detecting weak signals obscured by strong interferences, a challenge prevalent in diverse applications. For instance, in radio astronomy, observed celestial signals are inherently weak due to immense propagation distances, attenuation, and scattering by interstellar media [1]. These faint signals are often masked by strong interferences from known terrestrial and spaceborne transmitters, such as satellite downlinks and cellular base station signals [2]. While the frequencies of these interferences are typically known due to prior awareness about the transmitters, their amplitudes remain uncertain, influenced by factors such as varying propagation distances, atmospheric conditions, and multipath effects [3]. In addition, such interferences are often significantly strong in amplitude compared to the faint signals of interest and can easily exceed the dynamic range of the analog-to-digital converter (ADC) in the sensitive radio astronomy receiver, leading to saturated observations [2], [4]. The rapid expansion of satellite mega-constellations, operating at non-linear amplifier regions exacerbates these issues by emitting high-power interferences [5]. Using these saturated observations, conventional spectral estimators fail to accurately capture the weak signals' spectrum, as the ADC saturation phenomenon introduces non-linear distortions that randomly alter the overall signal structure [6], [7].

This work was supported in part by the National Science Foundation under grants CCF-2316865, ECCS-1923739, ECCS-2212940, and ECCS-23325341.

Traditional solutions, such as enforcing radio quiet zones, can mitigate terrestrial interference but fail to address dynamic and unpredictable satellite-induced interferences [8]. Additionally, enhancing receiver dynamic ranges with high-resolution ADCs is often costly and impractical due to increased data rates and storage demands [9]. These challenges underscore the need for innovative solutions that balance performance and feasibility.

In this paper, we consider the challenge of estimating weak signals amidst strong interferences with known frequencies but unknown amplitudes. We introduce a novel framework for spectral estimation that combines modulo sampling, interference cancellation (IC) technique, and adaptive spectral estimators. Modulo sampling uses a folding ADC sampler that generates folded observations by confining signals within the dynamic range [10]. A reconstruction framework introduced in [11], can be employed to recover the original signal from modulo samples. Following reconstruction, an orthogonal projection-based IC is applied to effectively suppress interferences, enabling conventional fast Fourier transform (FFT) for weak signal estimation. Additionally, adaptive estimators like amplitude and phase estimation of a sinusoid (APES) and Capon are utilized to deliver enhanced high-resolution spectral analysis, exploiting their adaptivity, superior sidelobe suppression, and interference handling capabilities [12].

Numerical simulations affirm the proposed framework's effectiveness, showing that modulo-sampling achieves spectral estimates nearly identical to the true spectrum while significantly outperforming conventional methods with saturated samples. Notably, APES and Capon estimators demonstrate inherent interference-handling capabilities, successfully detecting weak signals even without IC, thereby simplifying the framework [13]. The simulations further highlight a reduced mean-squared error (MSE) in the amplitude estimation of weak signals. These findings validate the framework's potential to address real-world challenges in spectral estimation, such as those encountered in radio astronomy.

II. Data Model and Problem Formulation

Consider a signal $y(t)$ comprising K weak signals, L strong interferences, and an additive noise given by

$$y(t) = \sum_{k=1}^{K} \alpha_k e^{j\omega_k t} + \sum_{l=1}^{L} \alpha_l e^{j\omega_l t} + w(t), \qquad (1)$$

where α_k and α_l denote the complex amplitude of the k-th signal of interest and the l-th interference respectively, while ω_k and ω_l denote their respective frequencies. The term $w(t)$ accounts for the additive noise. The interferences are assumed to dominate the weak signals, i.e., $|\alpha_l| \gg |\alpha_k| \ \forall \ k, l$. Furthermore, the interference frequencies ω_l are considered known, whereas their amplitudes α_l remain unknown. We aim to estimate the spectral content of the weak signals in the presence of such dominant interferences and additive noise. To solve the spectral estimation problem, the first step is to convert (1) to digital form via a sampler. We begin with an ideal sampler, which provides an optimal benchmark for subsequent conventional samplers.

A. Ideal Sampler

An ideal sampler captures N samples from (1) with a sufficiently high sampling rate $f_s = \frac{1}{T_s}$ to satisfy the Nyquist criterion. The resulting discrete-time observations can be expressed as

$$y[n] = \sum_{k=1}^{K} \alpha_k e^{j\omega_k n T_s} + \sum_{l=1}^{L} \alpha_l e^{j\omega_l n T_s} + w(nT_s), \quad n = 0, 1 \dots N-1. \tag{2}$$

This formulation assumes an ideal sampler that preserves the signal's full dynamic range without saturation or clipping. While useful as a theoretical benchmark for comparison, it overlooks real-world limitations like ADC saturation and resolution constraints.

B. Saturation Effect in Conventional Sampling

Unlike an ideal sampler, conventional samplers have a limited dynamic range and clip input signals that exceed a specified amplitude threshold λ. For an input signal $y(t)$, the corresponding output sequence from the sampler is

$$y_{\text{sat}}[n] = \begin{cases} \lambda; & y[nT_s] > \lambda \\ y[nT_s]; & -\lambda \le y[nT_s] \le \lambda, \\ -\lambda; & y[nT_s] < -\lambda \end{cases} \tag{3}$$

where $\{y_{\text{sat}}[n]\}$ is a N length sequence saturated at the threshold λ. Saturation introduces nonlinear distortion to the signal, resulting in flat-top shapes in regions where amplitude exceeds the ADC's threshold λ, as shown in Fig. 1.

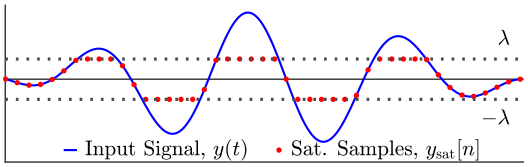

Fig. 1: Input signal and saturated (sat.) samples from the conventional sampler.

This distortion poses significant challenges for spectral analysis, as it alters the signals' overall structure and introduces phase inconsistencies. In such scenarios, IC methods may fail to reject interferences due to the nonlinear modifications caused by saturation.

Moreover, strong interference in the spectral domain leads to leakage, manifesting as sidelobes. This leakage results from the inherent spectral spreading caused by the window function's frequency response, where high-energy interference signals generate significant sidelobes that can mask weaker signals. The masking effect for the k-th weak signal is given by

$$P_{\text{m}}(\omega_k) = \sum_{l=1}^{L} |\alpha_l|^2 \left| \frac{\sin\left(\pi T_s(\omega_k - \omega_l)\right)}{\pi T_s(\omega_k - \omega_l)} \right|^2, \tag{4}$$

where $P_{\text{m}}(\omega_k)$ represents the power of interference sidelobes affecting the weak signal. Given that $|\alpha_l| \gg |\alpha_k|$, the masking power typically dominates, i.e.,

$$P_{\text{m}}(\omega_k) > |\alpha_l|^2 \tag{5}$$

and overshadows the weak signals, making it difficult to detect them when their frequency components overlap with the interference sidelobes.

The problem of interest is to estimate the spectral contents of the weak signals, α_k and ω_k for $k = 1, 2 \dots K$, in the presence of strong interference that may potentially exceed the ADC's dynamic range.

III. Proposed Approach

The impact of saturation cannot be directly handled by traditional methods. In this section, we propose a novel approach to spectral estimation incorporating modulo sampling with an IC scheme. Modulo-sampling technique folds the input signal within an accepted range to avoid saturation. After accurate reconstruction, the IC scheme successfully rejects interferences as the reconstructed data closely aligns with the full dynamic range observations. Applying IC eventually unmasks the weak signals from the sidelobes of interferences. It will be shown that FFT with IC can estimate the weak signals whereas APES and Capon can directly estimate the spectrum without IC due to their inherent interference handling capability.

A. Modulo Sampling and Reconstruction

Modulo sampling and reconstruction approach presented at [11], [14] introduces self-reset ADC that constrain the input signal within the dynamic range of ADC $[-\lambda, \lambda]$, avoiding saturation. The folding operation is described by

$$\mathscr{M}_\lambda : y(t) \to y_\lambda(t) = 2\lambda \left(\left[\!\!\left[\frac{y(t)}{2\lambda} + \frac{1}{2} \right]\!\!\right] - \frac{1}{2} \right), \tag{6}$$

where $[\![x]\!] = x - \lfloor x \rfloor$ defines the fractional part of x and we define $\mathscr{M}_\lambda$ as the modulo folding operator. This approach folds $y(t)$ back within $[-\lambda, \lambda]$ as shown in (6). A conventional sampler then samples the folded signal, producing modulo samples $\{y_\lambda[n]\}$ without saturation. Modulo samples can be reconstructed back to $\{\hat{y}[n]\}$ through a reconstruction process

presented at Algorithm 1. The reconstructions start with computing $\mathcal{D}$-th order finite difference of the modulo observations $\Delta^{\mathcal{D}} y_\lambda[n]$, where the first-order difference is

$$\Delta y_\lambda[n] = y_\lambda[n+1] - y_\lambda[n]. \tag{7}$$

Higher-order differences are recursively computed as

$$\Delta^{\mathcal{D}} y_\lambda = \Delta^{\mathcal{D}-1}(\Delta y_\lambda), \tag{8}$$

with the required difference order $\mathcal{D}$ determined by

$$\mathcal{D} = \left\lceil \frac{\log \lambda - \log \beta_g}{\log(T_s \Omega e)} \right\rceil, \tag{9}$$

where β_g is an upper bound of $y(t)$, Ω is the maximum frequency content, and e is Euler's constant. Then we compute the residual error $\Delta^{\mathcal{D}}\epsilon_r[n]$ caused by the modulo operation on the $\Delta^{\mathcal{D}} y_\lambda[n]$, which quantifies the correction needed to unwrap the original signal. The reconstruction involves applying an anti-difference operation $\mathscr{S}$ to the residual $\Delta^{\mathcal{D}}\epsilon_r[n]$, defined at the n-th element of a sequence $\{s[n]\}$ as

$$\mathscr{S} : \{s[n]\} \to \sum_{m=0}^{n-1} s[m] = s[0] + \cdots + s[n-1], \tag{10}$$

where $\mathscr{S}$ is the anti-difference operator. This reverses the effect of finite differencing and initiates unwrapping the folded signal. The resulting value is adjusted to the nearest multiple of 2λ, mitigating nonlinearities from the modulo operation. Subsequently, a correction factor $2\lambda\kappa_i$ is added for further alignment with the original signal, with κ_i computed using a second order anti-difference operation on the residual error, $\mathscr{S}^2(\Delta\epsilon_r)[n]$. The iterative approach runs up to $\mathcal{D}-1$ times to reconstruct the signal. A graphical manifestation of this process is shown in Fig. 2.

Algorithm 1 Recovery from Folded Samples [11]

Input: $y_\lambda[n]$, β_g and λ
Output: $\hat{y}[n]$
(1) Compute $\mathcal{D} = \left\lceil \frac{\log\lambda - \log\beta_g}{\log(T_s\Omega e)} \right\rceil$
(2) Compute $(\Delta^{\mathcal{D}} y_\lambda)[n]$
(3) Compute $(\Delta^{\mathcal{D}}\epsilon_r)[n] = \left(\mathscr{M}_\lambda(\Delta^{\mathcal{D}} y_\lambda) - \Delta^{\mathcal{D}} y_\lambda\right)[n]$
Set $s_0[n] = (\Delta^{\mathcal{D}}\epsilon_r)[n]$
for $i = 0 : \mathcal{D} - 2$ **do**
i) $s_{(i+1)}[n] = (\mathscr{S} s_{(i)})[n]$
ii) $s_{(i+1)} = 2\lambda \left\lceil \frac{\left\lfloor \frac{s_{(i+1)}}{\lambda} \right\rfloor}{2} \right\rceil$
iii) Compute $\kappa_i = \left\lfloor \frac{(\mathscr{S}^2\Delta^i\epsilon_r)[1] - (\mathscr{S}^2\Delta^i\epsilon_r)[\frac{6\beta_g}{\lambda}+1]}{12\beta_g} + \frac{1}{2} \right\rfloor$
iv) $s_{(i+1)}[n] = s_{(i+1)}[n] + 2\lambda\kappa_i$
end for
(4) $\hat{y}[n] = \mathscr{S} s_{(\mathcal{D}-1)}[n] + y_\lambda(n) + 2\lambda p,\ p \in \mathbb{Z}$

The reconstructed samples $\{\hat{y}[n]\}$ closely align with the ideal samples $\{y[n]\}$ and they can be processed using IC techniques such as orthogonal projection to remove interference contributions. This integrated approach facilitates signal recovery and spectral analysis of weak signals.

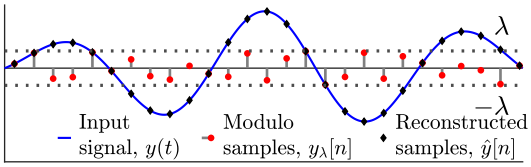

Fig. 2: Visualization of modulo sampling and reconstruction.

B. Orthogonal Projection-based IC

According to [15], observations such as $y[n]$ from (2) can be presented in the matrix form as

$$\boldsymbol{y} = \mathbf{A}_k\boldsymbol{\alpha}_k + \mathbf{A}_l\boldsymbol{\alpha}_l + \boldsymbol{w}, \tag{11}$$

where $\mathbf{A}_k = [\boldsymbol{a}_k(\omega_1) \quad \boldsymbol{a}_k(\omega_2) \ \ldots \ \boldsymbol{a}_k(\omega_K)]_{N\times K}$ and $\mathbf{A}_l = [\boldsymbol{a}_l(\omega_1) \quad \boldsymbol{a}_l(\omega_2) \ \ldots \ \boldsymbol{a}_l(\omega_L)]_{N\times L}$ are the matrices consisting of the steering vectors for signals and interferences with each column defined as $\boldsymbol{a}_k(\omega) = \boldsymbol{a}_l(\omega) = [1 \ e^{j\omega} \ \ldots \ e^{j(N-1)\omega}]^{\mathrm{T}}$ at ω frequency. The vectors $\boldsymbol{\alpha}_k = [\alpha_1 \ \alpha_2 \ \ldots \ \alpha_K]^{\mathrm{T}}$ and $\boldsymbol{\alpha}_l = [\alpha_1 \ \alpha_2 \ \ldots \ \alpha_L]^{\mathrm{T}}$ contain the respective complex amplitudes, with $(.)^{\mathrm{T}}$ is the matrix transpose operator and $\boldsymbol{w}$ is an $N \times 1$ noise vector. To remove interference, an orthogonal projection is applied to eliminate components in the subspace spanned by $\mathbf{A}_l$ defined as

$$\mathbf{P}_l^{\perp} = \mathbf{I}_N - \mathbf{A}_l \left(\mathbf{A}_l^{\mathrm{H}}\mathbf{A}_l\right)^{-1} \mathbf{A}_l^{\mathrm{H}}, \tag{12}$$

where $\mathbf{I}_N$ is a $N \times N$ dimensional identity matrix and $(.)^{\mathrm{H}}$ denotes the Hermitian transpose. Applying $\mathbf{P}_l^{\perp}$ to the observed signal $\boldsymbol{y}$ yields

$$\boldsymbol{y}_0 = \mathbf{P}_l^{\perp}(\mathbf{A}_k\boldsymbol{\alpha}_k + \mathbf{A}_l\boldsymbol{\alpha}_l + \boldsymbol{w}) = \mathbf{P}_l^{\perp}(\mathbf{A}_k\boldsymbol{\alpha}_k + \boldsymbol{w}), \tag{13}$$

where $\mathbf{P}_l^{\perp}\mathbf{A}_l\boldsymbol{\alpha}_l = 0$ due to orthogonality. The result is an interference-free signal, $\boldsymbol{y}_0$, containing only the weak signals and noise for spectral analysis.

C. Adaptive Spectral Estimators

Spectral analysis can be carried out with conventional FFT-based estimation or adaptive spectral estimators like APES and Capon. We apply the Capon and APES estimators for spectral estimation as described at [16]. Let

$$\begin{aligned} \boldsymbol{y}[u] &= \begin{bmatrix} y[u] & y[u+1] & \ldots & y[u+M-1] \end{bmatrix}^{\mathrm{T}} \\ u &= 0, 1 \ldots U-1, \end{aligned} \tag{14}$$

be the overlapping vectors from data $\{y[n]\}$, where M is the filter length with $U = N - M + 1$. By examining one frequency component at a time, Capon and APES determine the signal spectrum by scanning through the entire frequency band. To this end, the signal can be expressed as

$$\boldsymbol{y}[u] = [\alpha(\omega)\boldsymbol{a}_M(\omega)]e^{j\omega u} + \boldsymbol{w}_\omega[u], \tag{15}$$

where ω is the current frequency component and $\alpha(\omega)$ denotes its unknown complex amplitude, while $\boldsymbol{w}_\omega[u]$ contains the contributions from frequencies other than ω plus noise.

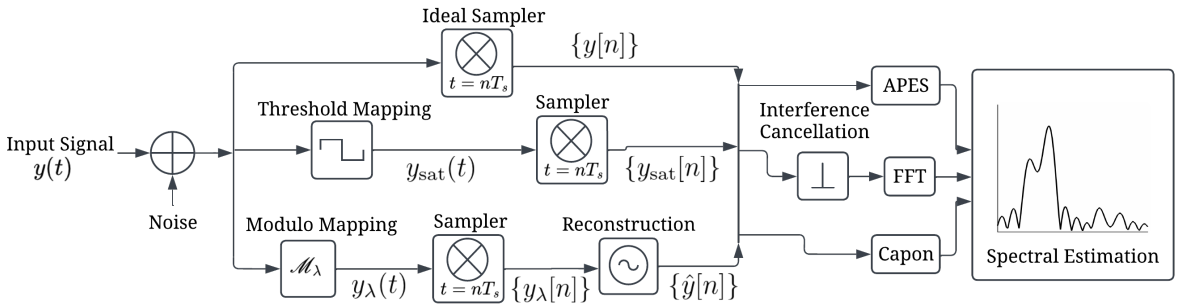

Fig. 3: Proposed spectral estimation framework using modulo sampling, benchmarked against ideal and conventional samplers.

Adaptive spectral estimators use a matched filter bank (MAFI) designed to maximize the signal-to-noise ratio (SNR) at the output. The solution of this optimization problem is

$$\boldsymbol{h}_\omega = \frac{\mathbf{Q}^{-1}(\omega)\boldsymbol{a}_M(\omega)}{\boldsymbol{a}_M^{\mathrm{H}}(\omega)\mathbf{Q}^{-1}(\omega)\boldsymbol{a}_M(\omega)}, \tag{16}$$

where $\mathbf{Q}(\omega)$ is the noise covariance matrix. The solution ensures $\boldsymbol{h}_\omega^{\mathrm{H}}\boldsymbol{a}_M(\omega) = 1$, keeping the frequency components undistorted. One least-square estimate of $\alpha(\omega)$ from (16) is

$$\hat{\alpha}(\omega) = \boldsymbol{h}_\omega^{\mathrm{H}}\boldsymbol{g}(\omega), \tag{17}$$

where $\boldsymbol{g}(\omega)$ is the normalized Fourier transforms of the data vector given by

$$\boldsymbol{g}(\omega) = \frac{1}{U}\sum_{u=0}^{U-1}\boldsymbol{y}[u]e^{-j\omega u}. \tag{18}$$

Equation (17) is a general amplitude estimation framework of MAFI estimators. APES and Capon estimates are derived by substituting different noise covariance matrix estimates into (16). The resulting estimate for Capon can be expressed as

$$\hat{\alpha}_{\text{Capon}}(\omega) = \frac{\boldsymbol{a}_M^{\mathrm{H}}(\omega)\hat{\mathbf{R}}^{-1}\boldsymbol{g}(\omega)}{\boldsymbol{a}_M^{\mathrm{H}}(\omega)\hat{\mathbf{R}}^{-1}\boldsymbol{a}_M(\omega)}, \tag{19}$$

where the sample covariance matrix $\hat{\mathbf{R}}$ is estimated as

$$\hat{\mathbf{R}} = \frac{1}{U}\sum_{u=0}^{U-1}\boldsymbol{y}[u]\boldsymbol{y}^{\mathrm{H}}[u]. \tag{20}$$

APES estimate is similar to Capon except that $\hat{\mathbf{R}}$ is replaced by $\hat{\mathbf{Q}}$

$$\hat{\alpha}_{\text{APES}}(\omega) = \frac{\boldsymbol{a}_M^{\mathrm{H}}(\omega)\hat{\mathbf{Q}}^{-1}(\omega)\boldsymbol{g}(\omega)}{\boldsymbol{a}_M^{\mathrm{H}}(\omega)\hat{\mathbf{Q}}^{-1}(\omega)\boldsymbol{a}_M(\omega)}, \tag{21}$$

where $\hat{\mathbf{Q}}$ the estimate of noise covariance is given by $\hat{\mathbf{Q}} = \hat{\mathbf{R}} - \boldsymbol{g}(\omega)\boldsymbol{g}^{\mathrm{H}}(\omega)$. Both APES and Capon estimates are derived considering ideal samples but applicable to saturated and modulo samples, maintaining a similar structure.

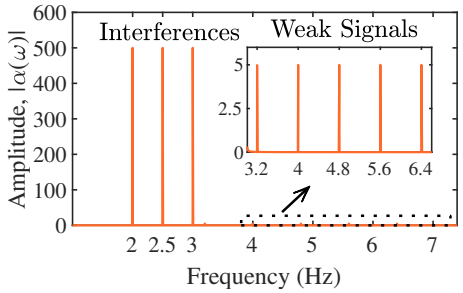

Fig. 4: True spectrum of the 1-D dataset.

D. Summary of the Proposed Approach

The proposed framework addresses strong interference and saturation constraints in spectral estimation by integrating modulo sampling, orthogonal projection-based IC method, and adaptive spectral estimators. Modulo sampling avoids saturation by folding signals within a predefined range, and a reconstruction algorithm restores the original data. The reconstructed signal is then processed using an orthogonal projection method to cancel known interferences effectively. Finally, high-resolution estimators like Capon and APES are applied for spectral analysis, while FFT with IC serves as a benchmark. A schematic understanding of our approach is depicted in Fig. 3.

IV. Numerical Analyses

A. Simulation Settings

The dataset comprises 3 strong interferences having amplitudes $\boldsymbol{\alpha}_l = [500e^{\frac{j\pi}{4}}\ 500e^{\frac{j\pi}{4}}\ 500e^{\frac{j\pi}{4}}]^{\mathrm{T}}$ and frequencies $\boldsymbol{f}_l = [2\ 2.5\ 3]^{\mathrm{T}}$ Hz. Moreover, amplitudes and frequencies of 5 weak signals are $\boldsymbol{\alpha}_k = [5e^{\frac{j\pi}{4}}\ 5e^{\frac{j\pi}{4}}\ \ldots\ 5e^{\frac{j\pi}{4}}]^{\mathrm{T}}$ and $\boldsymbol{f}_k = [3.2\ \ 4\ \ 4.8\ \ 5.6\ \ 6.4]^{\mathrm{T}}$ Hz, respectively. Here, the observations are corrupted by a zero-mean complex white Gaussian noise maintaining 0 dB SNR with the weak signals. Here, SNR at the k-th weak signal is defined as

$$\text{SNR}_k = 10\log_{10}\frac{\alpha_k^2}{P_e(\omega_k)}(\text{dB}), \tag{22}$$

where $P_e(\omega_k)$ is the spectral density of the additive noise at frequency ω_k. The true spectrum of the weak sinusoidal signals and interferences is shown in Fig. 4.

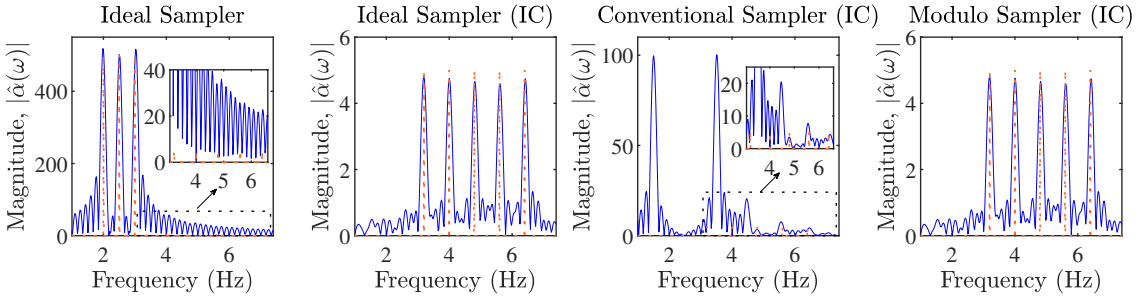

(a) FFT spectral estimates.

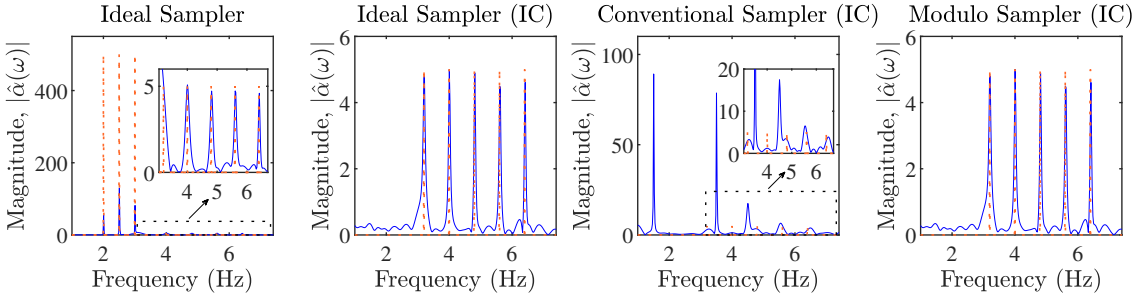

(b) Capon spectral estimates with filter length $M = 128$.

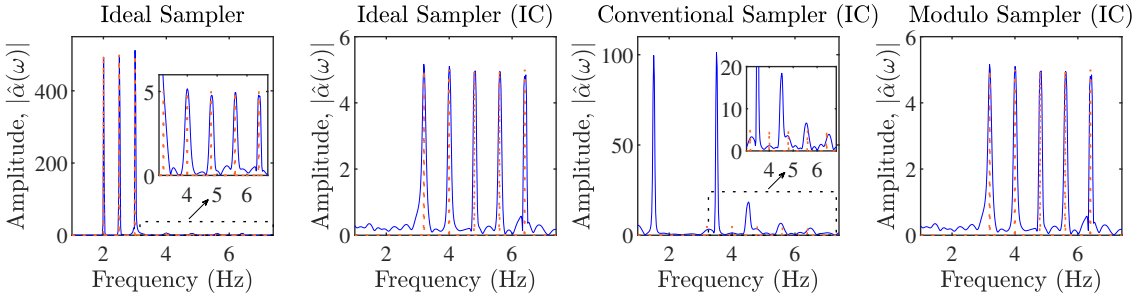

(c) APES spectral estimates with with filter length $M = 128$.

Fig. 5: Spectral estimates compared with the true spectrums across different observation-estimator categories.

In the subsequent analysis, we consider three samplers, the ideal sampler without dynamic range limitation (Section II-A), the conventional sampler that clips signals exceeding a specified threshold (Section II-B), and a modulo sampler that folds any out-of-range signals back into the dynamic range (Section III-A). The dynamic range for both the conventional and modulo samplers is $[-450, 450]$. For spectral estimation, we employ both the FFT-based approach and the adaptive spectral estimators Capon and APES as introduced in Section III-C. Finally, to examine the impact of the interference, we compare the performance of each sampler-estimator combination with and without an IC step. We use $N = 512$ samples for all these configurations and set the filter length M to 128 for Capon and APES to balance spectral resolution and accuracy. This multi-faceted setup enables a thorough investigation of how different samplers, estimators, and IC strategies influence the ability to estimate weak signals.

B. Results and Discussions

At first, we evaluate one-time spectral estimation results for each sampler-estimator category as presented in Fig. 5, where the rows are representatives of FFT, Capon, and APES estimators respectively. For each estimator, we arrange spectral estimates obtained from observations of the ideal sampler (without and with IC, respectively), the conventional sampler (with IC), and the modulo sampler (with IC) in the columns of Fig. 5. Additionally, we include a magnified portion of the weak signals' region as an inset in the 1st and 3rd column of Fig. 5 for clearer visualization.

In terms of performance, looking at FFT (1st row), the ideal sampler without IC (1st column) fails to recover the weak signals masked by the sidelobes of the strong interference signals. Applying IC (2nd column) eliminates the interferences, leading to accurate spectral estimates using the ideal sampler. However, with a conventional sampler (3rd column), saturation nonlinearly distorts the signal and IC cannot remove the interference effectively, producing random and erroneous spectra. In contrast, modulo sampler avoids saturation via folding, allowing IC to reveal the true spectrum (4th column).

Almost similar trade-offs are observed for Capon (2nd row) and APES (3rd row), except that APES and Capon exhibit their inherent interference handling capability and recover

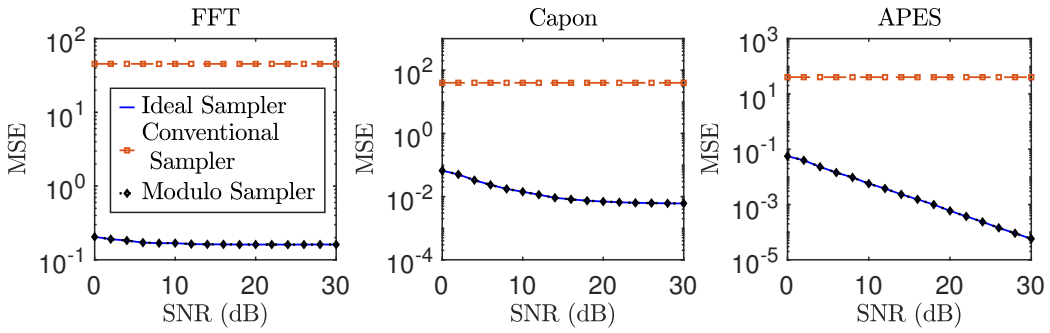

Fig. 6: Statistical evaluation of spectral estimates across different observation-estimator categories.

weak signals even without IC (1st column). This demonstrates that APES and Capon can simplify the proposed framework by eliminating the need for IC. The remaining scenarios are comparable to FFT: when the signal is saturated (3rd column), both estimators again yield false spectra, which again demonstrates the negative impact of saturation in spectral estimation. Avoiding saturation through our proposed framework enables these adaptive estimators to achieve enhanced estimates (4th column).

Among the three spectral estimators, FFT exhibits high sidelobes and somewhat less accurate peak heights (1st row). Capon enhances spectral resolution with narrower peaks but underestimates peak amplitudes (2nd row), a known characteristic of the method [16]. APES outperforms both, delivering the most accurate peak heights while maintaining slightly wider spectral peaks than Capon (3rd row).

Secondly, we present a statistical analysis using the mean squared error (MSE) of amplitude estimation across three estimator-sampler categories for the second weak signal across SNR levels from 0 to 30 dB. Specifically, let α_k be the true amplitude of the k-th weak signal, and let $\hat{\alpha}_k^{(i)}$ be its estimate during the i-th trial. We define the MSE as

$$\mathrm{MSE}(\hat{\alpha}_k) = \frac{1}{\eta}\sum_{i=1}^{\eta}\left|\hat{\alpha}_k^{(i)} - \alpha_k\right|^2, \tag{23}$$

where $\eta = 1000$ is the total number of iterations at each SNR level. In our simulations, we vary the SNR and evaluate MSE using (23) for each configuration with IC and the outcomes are presented in Fig. 6 using the log scale. Estimates using saturated samples result in significantly higher MSE for all three estimators. However, the modulo sampler achieves consistently low MSE levels, comparable to those of the ideal sampler. Even at 0 dB SNR, the framework demonstrates remarkable accuracy, proving its reliability in noisy conditions. The MSE analysis further strengthens the claim of using modulo samples in estimating weak signals with strong interferences.

V. Conclusion

This paper presents a 1-D spectral estimation framework under strong interference potentially leading to saturated observations. We provide a comparison between the proposed approach with modulo sampling and the conventional approach with saturated samples through statistical and deterministic analyses. Both types of results support the superiority of the proposed approach as the saturated observations tend to generate false and random spectra. This work offers a reliable solution for weak signal detection, with future efforts directed toward extending the framework for 2-D spectral estimations.

References

[1] G. B. Rybicki and A. P. Lightman, *Radiative Processes in Astrophysics*. New York, NY: Wiley, 1985.

[2] W. A. Baan, "Implementing RFI mitigation in radio science," *Journal of Astronomical Instrumentation*, vol. 08, no. 01, p. 1940010, 2019.

[3] A. R. Thompson, J. M. Moran, G. W. Swenson Jr, A. R. Thompson, J. M. Moran, and G. W. Swenson, "Radio frequency interference," *Interferometry and Synthesis in Radio Astronomy*, pp. 787–808, 2017.

[4] W. van Driel, "Radio quiet, please! - protecting radio astronomy from interference," *Proceedings of the International Astronomical Union*, vol. 5, pp. 457–464, 06 2009.

[5] R. Massey, S. Lucatello, and P. Benvenuti, "The challenge of satellite megaconstellations," *Nature Astronomy*, vol. 4, no. 11, pp. 1022–1023, 2020.

[6] F. Esqueda, S. Bilbao, and V. Välimäki, "Aliasing reduction in clipped signals," *IEEE Transactions on Signal Processing*, vol. 64, no. 20, pp. 5255–5267, 2016.

[7] A. Farina and L. Ortenzi, "Effect of ADC and receiver saturation on adaptive spatial filtering of directional interference," *Signal Processing*, vol. 83, no. 5, pp. 1065–1078, 2003.

[8] R. J. Cohen, G. Delgado, E. Hardy, T. Hasegawa, and L.-Å. Nyman, *Radio-Quiet Zones*. Springer Netherlands, 2003, pp. 225–259.

[9] V. Zakharenko and et al., "Digital receivers for low-frequency radio telescopes UTR-2, URAN, GURT," *Journal of Astronomical Instrumentation*, vol. 05, no. 04, p. 1641010, 2016.

[10] W. Kester, *ADC Architectures VI: Folding ADCs*, Analog Devices, Inc., 2009, mT-025 Tutorial.

[11] A. Bhandari, F. Krahmer, and R. Raskar, "On unlimited sampling and reconstruction," *IEEE Transactions on Signal Processing*, vol. 69, pp. 3827–3839, 2021.

[12] Z.-S. Liu, H. Li, and J. Li, "Efficient implementation of Capon and APES for spectral estimation," *IEEE Transactions on Aerospace and Electronic Systems*, vol. 34, no. 4, pp. 1314–1319, 1998.

[13] P. Stoica and R. L. Moses, *Spectral Analysis of Signals*. Upper Saddle River, NJ, USA: Prentice Hall, 2005.

[14] A. Bhandari, F. Krahmer, and R. Raskar, "On unlimited sampling," in *2017 International Conference on Sampling Theory and Applications (SampTA)*, 2017, pp. 31–35.

[15] Y.-m. Wang, X.-p. Mao, H. Hong, J. Zhang, and Y.-m. Cui, "A generalized oblique projection filter with flexible parameter for interference suppression," *International Journal of Antennas and Propagation*, vol. 2015, no. 1, p. 320769, 2015.

[16] H. Li, J. Li, and P. Stoica, "Performance analysis of forward-backward matched-filterbank spectral estimators," *IEEE Transactions on Signal Processing*, vol. 46, no. 7, pp. 1954–1966, 1998.